

Atomic Structure and Special Reactivity Toward Methanol Oxidation of Vanadia Nanoclusters on TiO₂(110)

Luca Artiglia,[†] Stefano Agnoli,^{*,†} Andrea Vittadini,[§] Alberto Verdini,[‡] Albano Cossaro,[‡] Luca Floreano,[‡] and Gaetano Granozzi[†]

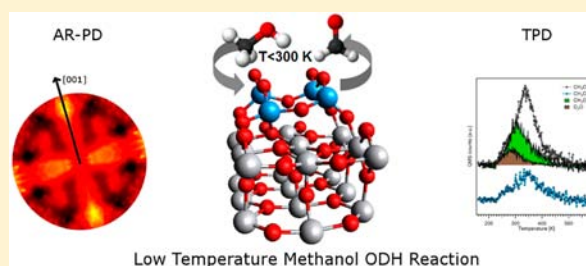
[†]Department of Chemical Sciences, University of Padua, I-35131 Padova, Italy

[§]ISTM-CNR, Via Marzolo 1, I-35131 Padova, Italy

[‡]CNR-IOM, TASC National Laboratory, I-34149, Trieste, Italy

S Supporting Information

ABSTRACT: We have grown highly controlled VO_x nanoclusters on rutile TiO₂(110). The combination of photoemission and photoelectron diffraction techniques based on synchrotron radiation with DFT calculations has allowed identifying these nanostructures as exotic V₄O₆ nanoclusters, which hold vanadyl groups, even if vanadium oxidation state is formally +3. Our theoretical investigation also indicates that on the surface of titania, vanadia mononuclear species, with oxidation states ranging from +2 to +4, can be strongly stabilized by aggregation into tetramers that are characterized by a charge transfer to the titania substrate and a consequent decrease of the electron density in the vanadium 3d levels. We then performed temperature programmed desorption experiments using methanol as probe molecule to understand the impact of these unusual electronic and structural properties on the chemical reactivity, obtaining that the V₄O₆ nanoclusters can selectively convert methanol to formaldehyde at an unprecedented low temperature (300 K).



INTRODUCTION

A complete understanding of the exceptional reactivity shown by monolayer vanadia/TiO₂ catalysts toward selective oxidations has eluded scientists for more than 30 years, despite the large amount of efforts devoted to this issue.^{1,2} Several different surface science experiments and quite sophisticated theoretical calculations have been carried out to study vanadia/TiO₂ nanostructures and the influence of the substrate on their reactivity, with the aim of developing efficient real catalysts established on a knowledge-based design.³ In particular, a fertile research area has focused on the understanding of the structure and reactivity of VO_x nanoclusters (hereafter VO_x-NCs)^{4–12} and ultrathin films^{13–17} supported on TiO₂(110). However, there is not yet a common view about the actual active catalytic sites and reaction mechanism.^{4,18,19}

The main reason for this impasse probably resides in the inadequate description of the real catalytic system. As a matter of fact, as we show in the present work, at the oxide/oxide interface the combination of structural constraints (i.e., the matching of two different lattices) and electronic interactions (i.e., local hybridization and charge transfer) determines the formation of unusual NCs, with no bulk or gas phase counterparts, which are characterized by special chemical properties. This indeed suggests that the new chemistry and physics already documented for ultrathin oxide films on metals²⁰ can be experienced also on oxide-on-oxide systems, and the study of these systems can lead to the identification of a

new family of nanostructures that can be used as a blueprint for the design of radically new molecular catalysts.²¹

Within this framework, the role of the oxide substrate is extremely relevant, since it can act both as a support to stabilize the active NCs and as an active “player”, thus affecting the overall system reactivity.²² For example, Ganduglia-Pirovano et al.²³ identified by density functional theory (DFT) calculations a synergy between VO_x monomers and the CeO₂(111) support, due to a VO_x→CeO₂ electron transfer that leads to the formation of Ce³⁺ defects, whereas V remains highly oxidized (V⁵⁺), and this interaction is at the basis of its high chemical reactivity. On the other hand, in the case of the CeO_x/TiO₂(110) system, ceria is stabilized in its reduced form (Ce³⁺) by the substrate, since the Ce 4f levels, as a result of the mixing with the O 2p band of titania, are stabilized at an energy below the Ti 3d states.^{24,25} In the case of vanadia monomers on TiO₂(110), DFT calculations indicate a constant charge on vanadium atom, close to 2+, on changing oxygen content from VO to VO₄.⁵ An analogous result was also obtained by the same authors in the case of vanadia supported on CeO₂(111) in contrast with ref 23. The origin of this discrepancy can be identified in the different theoretical approach used (GGA⁵ vs GGA+U²³) for the calculations. In particular, the description of localized defects in oxides requires an explicit treatment of the

Received: May 22, 2013

Published: October 25, 2013

electron interactions; however, also for very simple cases like, e.g., oxygen vacancy energy formation,²⁶ the choice of the U value is a critical parameter, which deeply impacts the total energy of the system. In any case, these exemplary cases illustrate the large variability in the role of the substrate, which can either stabilize reduced or oxidized states or even pinning a benchmark charge in the supporting oxide.

From the experimental point of view, Biener et al. deposited increasing amount of V on TiO₂(110) at room temperature in an oxygen environment, obtaining V₂O₃ islands that have a small interaction with the substrate. The islands grow in a disordered fashion and coalesce after thermal treatment to cover completely the substrate. No TiO₂ reduction was reported after V₂O₃ deposition.¹³ However, in the case of VO_{*x*}/TiO₂ powder catalysts, electron paramagnetic resonance measurements^{27,28} indicate the formation of Ti³⁺ species after catalytic work during oxidative dehydrogenation of propane, pointing once again to an active role of the substrate.

In a recent work, Paier et al.²⁹ investigated the structure and stability of VO_{*x*} NCs supported on CeO₂(111) and found that V₃O₆ trimers are the most stable species over a wide range of oxygen chemical potential. However, the huge diffusion barrier (higher than 1.95 eV)²⁹ experienced by VO₂ mononuclear clusters prevents aggregation at room temperature. The evaluation of the reactivity of these submonolayer VO_{*x*} NCs based on DFT calculations of the oxygen defect formation and hydrogenation energies has revealed that VO₂ monomers and dimers are the most active species³⁰ On the contrary, the reactivity is quenched by a further increase in the NC nuclearity, thus establishing an inverse correlation between thermodynamic stability and reactivity.³⁰

On the other hand, a combined experimental and theoretical investigation has revealed that VO_{*x*} NCs deposited on a nonreducible oxide like silica tend to aggregate into molecular structures, once again pointing out the role of the substrate in the NC stabilization.³¹ In the case of vanadia supported on different alumina surfaces, dimers are the only stable species on α -Al₂O₃(0001) at low coverage,³² whereas on κ -Al₂O₃(0001) the surface phase diagram is more complex and comprises the formation of monomers, dimers, trimers, and 1D rows for increasing V chemical potential.³² Besides on ultrathin alumina films grown on NiAl, taller clusters are formed.³³ Therefore, these studies show that variation in the atomic structure of the alumina substrate have a deep influence on the catalytic properties of the clusters by affecting the energy of oxygen vacancy formation.

In the present study, we used photoelectron spectroscopy (XPS), angle resolved photoelectron diffraction (AR-PD), and DFT calculations to provide a complete description of the atomic and electronic structure of VO_{*x*}-NCs on TiO₂ rutile-(110) in the submonolayer regime (~ 0.3 ML). Interestingly, in agreement with previously cited works,³⁰ we found that vanadia species are not stable as single monomeric units, whereas the aggregation into polynuclear NCs is highly favored. This behavior has been already documented in other nano-oxides like ceria dimers,^{24,25} RuO_{*x*} nanochains,³⁴ FeO_{*x*}-NCs,³⁵ WO₃ trimers³⁶ on TiO₂, or VO_{*x*} oligomers on ceria³⁷ or ZrO₂^{38,39} and TiO₂.¹⁰ This result indicates that, as opposed to previous investigation of vanadia/TiO₂ catalysts focusing either on continuous epitaxial thin films^{17,13,40} or monatomic clusters,^{7,41,42} also this intermediate regime, characterized by aggregation at the nanoscopic level, can be of pivotal

importance for the definitive comprehension of real catalytic systems.

In the present work, we combined structural characterization with reactivity studies by carrying out temperature programmed desorption (TPD) experiments. Methanol has been used as a probe molecule not only because of its simplicity and common use in surface science investigations⁴³ but also for the great interest of its chemistry in different fields.^{44–46} Interestingly, we found that the VO_{*x*}-NCs on TiO₂(110) are excellent catalyst toward the low-temperature (LT) methanol oxidative dehydrogenation (MODH) reaction: methanol can be converted to formaldehyde with very high selectivity at unprecedented low temperature (300 K).

RESULTS AND DISCUSSION

To obtain the VO_{*x*}/TiO₂(110) model system, we evaporated 0.3 ML of metallic V in an oxygen background. According to previously reported scanning tunneling microscopy (STM) data (see also Figure S1),⁴⁷ this procedure allows depositing highly controlled VO_{*x*}-NCs (white circles) that grow on top of the 5-fold coordinated Ti rows (Ti_{5c}).⁴⁸ In the present case, we used a slightly higher oxygen partial pressure (5.0×10^{-8} mbar) than in ref 47 (1.0×10^{-8} mbar), in order to promote a better VO_{*x*}-NCs oxidation. The dark circles in Figure S1 point out the presence of TiO_{*x*} reconstructions that have been already observed in similar preparation conditions.⁴⁹

Figure 1a shows the V 2p XPS data acquired with a photon energy of 650 eV after V deposition: the complex line shape suggests the presence of several components, thus in Figure 1b we report the separation of the V 2p_{3/2} photoemission line into single peaks, showing a low intensity component centered at a binding energy (BE) of 513.4 eV (typical of V^(II))^{50,51} related to partially oxidized NCs and the other two at 515.6 and 517.0 eV that can be attributed to the typical multiplet structure of vanadium oxides and are compatible with either V^(III) or V^(IV).^{52–54}

Some more insight on the electronic structure comes from the resonant photoemission spectra (RES-PES) of the valence band (VB), acquired scanning the photon energy across the V L_{2,3} absorption threshold (Figure 1c, right): the 2D plot shows a strong intensity variation (proportional to color brightness) of the peak close to the Fermi level (at ~ 1.2 eV) and of the broad band between 3 and 9 eV, as shown in Figure 1d, which reports a line profile corresponding to the VB in resonant conditions ($h\nu = 516.5$ eV). The former can be assigned to V 3d states and the latter mostly to the O 2p band, revealing therefore a strong hybridization between metal and oxygen states. These data suggest a population of V 3d band, excluding the presence of V^(V), in agreement with the V 2p photoemission peaks position and fwhm (Figure 1b).^{13,53,54}

To unravel the structure of the VO_{*x*}-NCs we carried out angle resolved photoelectron diffraction (AR-PD) experiments where the photoelectron intensity I is monitored as a function of the polar (θ) and azimuthal (φ) angles (see Experimental section). By this technique one can probe the arrangement of atoms around a selected emitter.⁵⁵ We consider the anisotropy function $\chi(\theta, \varphi) = I(\theta, \varphi)/(I_0(\theta) - 1)$, where $I_0(\theta)$ is the average evaluated from $I(\theta, \varphi)$ over φ in the 0–360° range, and the plot of χ vs (θ, φ) is called anisotropy 2π pattern.⁵⁶ The presence of anisotropy is an indication of an ordered arrangement around the emitter.

The experimental 2π plot of the V 2p_{3/2} peak is reported in Figure 2a: we show only the intensity of the main oxidized

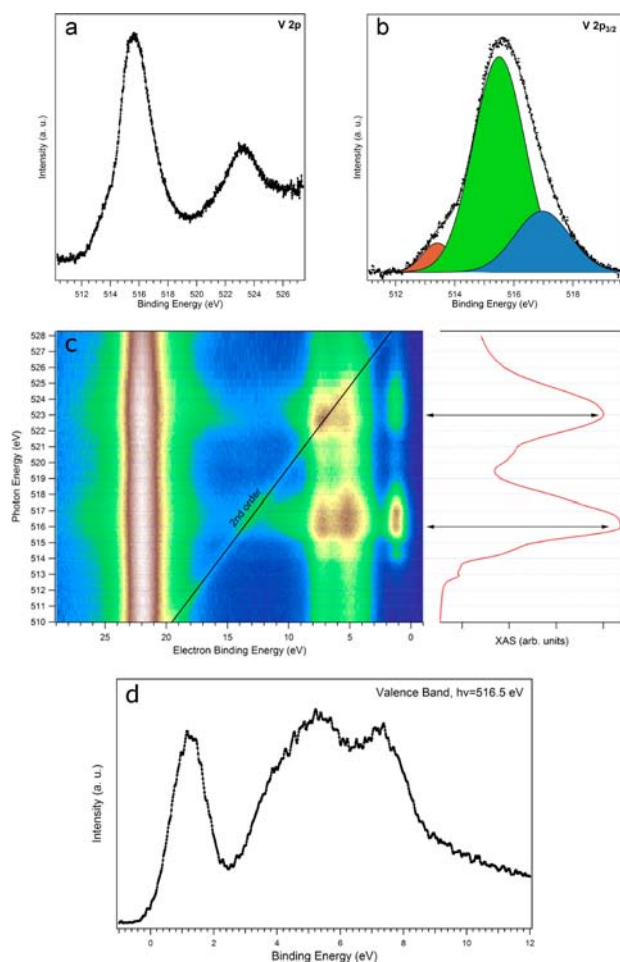


Figure 1. Photoemission data of (a) V 2p peaks collected immediately after 0.3 ML V deposition on TiO₂(110) taken with a photon energy of 650 eV; (b) V 2p_{3/2} peak separated in three components (see text); (c) RES-PES of the VB collected across the V L_{2,3} edge (see on the right). The black line in figure indicates the emission from Ti 2s level due to second order yield of the monochromator; (d) VB in resonant conditions ($h\nu = 516.5$ eV).

component centered at 515.6 eV (resulting in a photoelectron kinetic energy of 296 eV). Actually, after the separation into single components of each photoemission spectrum, we noticed that the component at 517 eV had the same pattern of the main one, while the one at 513.4 eV, associated to minority under-stoichiometric VO_x-NCs, presented an almost featureless anisotropy (i.e., a structural disorder). The reported 2π pattern displays two clear maxima aligned with the TiO₂ substrate [001] direction, ($\theta = 58^\circ$) due to forward scattering (FS) events caused by the O ions belonging to the NCs.

This is in well agreement with previous STM measurements showing that the NCs are aligned with the TiO₂ [001] crystallographic direction and centered on top of the Ti_{5c} rows.⁴⁷

Capitalizing on the whole set of these results, we simulated by DFT calculations a stable structure for VO_x-NCs growing on top of the Ti_{5c} rows and with a size compatible with the STM images (Figure S1, i.e., NC are about 6 Å wide along the [001] directions, see ref 47).

The properties of isolated mononuclear VO_x-NCs ($x = 1-4$) adsorbed on TiO₂(110) have been already studied by DFT calculations:⁴ for all the values of x , the VO_x-NCs are

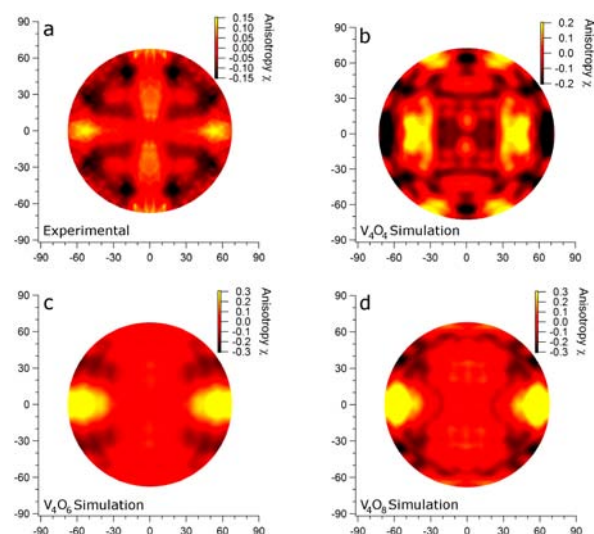


Figure 2. (a) Experimental AR-PD 2π pattern (kinetic energy of 296 eV); simulated AR-PD patterns for (b) V₄O₄, (c) V₄O₆, and (d) V₄O₈. The projection is linear in θ (surface normal at $\theta = 0^\circ$) in the center. The azimuth $\varphi = 0^\circ$ (90°) is found at 3 o'clock (12 o'clock) and corresponds to the [001] ([$\bar{1}\bar{1}0$]) direction.

asymmetrically adsorbed on one side of the bridging oxygen (O_{br}) rows,⁴⁸ with the V atom interacting with two O_{br} atoms and one/two O atoms bound to a Ti_{5c} (see also Figure S2 upper left). Since neither the location nor the size of such NCs are compatible with the STM images,⁴⁷ we deduce that we are dealing with polynuclear (V_yO_x , $y > 1$)VO_x-NCs. To investigate the tendency toward aggregation for NCs of different stoichiometry at the lowest computational cost, we fixed the surface coverage, expressed as the $n(V)/n(\text{Ti}_{5c})$ ratio, to 0.5 ML. This allowed us to model mono-, di-, and tetra-nuclear NCs with 1×2 , 1×4 , and 2×4 supercells, respectively. While the minimum energy structures result to be identical to those found in ref 6, the energetics is slightly different because of the smaller slab size (in literature a 1×4 supercell). This has the effect of destabilizing more oxidized NCs, so that using the GGA we compute $\Delta E = -3.39$ eV against -3.80 eV⁵ for the VO_(ads) + 1/2 O_{2(g)} → VO_{2(ads)} process, and $\Delta E = -1.06$ eV against -1.39 eV⁵ for the VO_{2(ads)} + 1/2 O_{2(g)} → VO_{3(ads)} process (the models corresponding to these structures are reported in Figure S2). These values decrease significantly (-2.45 and -0.58 eV, respectively) by adopting the GGA+U method, which alleviates the well-known self-interaction problem of the GGA functionals. However, in the following we will compare the stability of NCs with the same degree of oxidation, therefore this effect can be expected to be less important.

We started by examining the V₂O_x case: since at least one oxygen must be shared between V atoms, NCs of formula V₂O₅, V₂O₄, V₂O₃, V₂O₂, and V₂O can be proposed. We carefully explored the configuration space of these models by selecting and optimizing several configurations. We found that all the NCs prefer to bind to O_{br} rows similarly to the literature mononuclear VO_x models⁵ (see Figure S2) and are thus incompatible with the experiment. For this reason, we decided to explore the properties of V₄O_x-NCs, taking in consideration V₄O₄, V₄O₆, V₄O₈, and V₄O₁₀. Basically, V₄O₄, V₄O₆, and V₄O₈ can all be described as truncated V₂O₃ rows (see Figure S2), which are in turn modeled on the Ti₂O₃ rows proposed by Blanco-Rey et al. to describe the TiO₂(110)-(1 × 2)

reconstruction.⁵⁷ The V_4O_{10} NCs are structurally similar but are displaced by half a lattice constant along $[1\bar{1}0]$.

Both GGA and GGA+*U* calculations show that, with the exception of the highest oxidation state, tetranuclear NCs are stable against decomposition into both dinuclear and mononuclear NCs. In particular, GGA+*U* (GGA) ΔE s of the $V_4O_4 \rightarrow 4 VO$ and $V_4O_8 \rightarrow 4 VO_2$ processes are +0.17 (+0.52) eV/(V atom) and +0.20 (+0.77) eV/(V atom), respectively. At the same time, we find that for the $V_4O_{2x} \rightarrow V_2O_x$ processes GGA+*U* (GGA) ΔE s amount to +0.10 (+0.39), +0.04 (+0.18), +0.25 (+0.99), -0.14 (-0.58) eV/(V atom) on increasing *x* from 2 to 5 (see Figure 3 for *x* = 3 and 4).

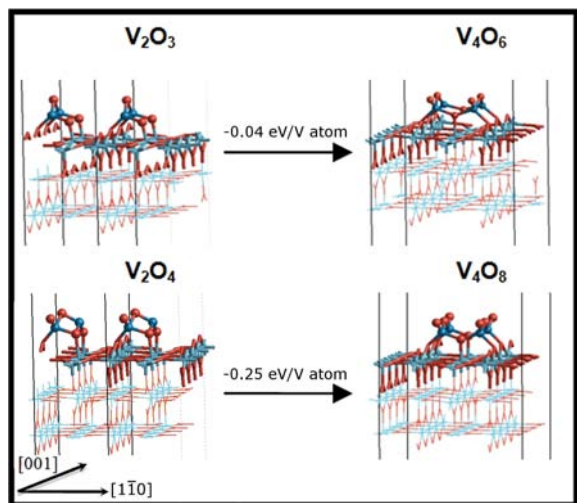


Figure 3. DFT simulations of dinuclear (left) and tetranuclear (right) V_xO_x -NCs for the $V^{(III)}$ and $V^{(IV)}$ oxidation states. The energy gain (eV/V atom) shows that the formation of tetranuclear NCs is favored.

Summarizing, if we define as Ti-centered and Ti-off the NCs that are centered atop the Ti_{sc} and relaxed toward the side of O_{br} rows respectively, DFT calculations predict that Ti-off mononuclear NCs are stable for VO_3 ,⁵⁸ whereas Ti-offset dinuclear NCs are stable for $V^{(V)}$, and Ti-centered tetra-nuclear NCs are preferred for lower V oxidation states. This result is remarkable since it reveals that at the nanoscale there is a strong tendency to form small aggregates quite different from the building blocks of bulk oxides, whose exotic structures can be the reason of their peculiar chemical activity. As already stated in the introduction, this behavior has been already reported in other VO_x nano-oxides grown on other substrates.^{23,29,31}

As mentioned above, the models for all the tetranuclear species can be ideally obtained by truncating V_2O_3 chains. In particular, converting half of the V–O–V bridges into two V=O groups yields V_4O_8 species, whereas removing half of the O bridges yields V_4O_4 species (see also Figure S2). The V_4O_6 species can be obtained if half of the V–O–V bridges are asymmetrically broken to V + V=O (Figure 3 upper right).

The AR-PD patterns simulated for the possible NC models (Figure 2b–d) have been compared to the experimental one (Figure 2a) via an *R*-factor analysis, and the results are reported in Table 1. On the basis of these AR-PD (Figure 2) and photoemission (Figure 1) results, the V_4O_4 model (Figure 2b) can be ruled out (in the following we will disregard it), as also demonstrated by a high *R*-factor value of 0.78. Both the remaining models (V_4O_6 and V_4O_8) have a very similar local

Table 1. *R*-Factors of the Different NC Models^a

| | V_4O_4 | V_4O_6 | V_4O_8 |
|------------------|----------|----------|----------|
| <i>R</i> -Factor | 0.78 | 0.42 | 0.45 |

^aThe V_4O_6 model has been symmetrized with respect to the substrate.

structure around the V ions and therefore cannot be discriminated only by means of AR-PD. Actually, Figure 2c,d present very similar 2π AR-PD plot simulations for the V_4O_6 and V_4O_8 structures: a cross-check with the experimental pattern in Figure 2a confirms a similar good agreement between the experimental data and the remaining NCs models, both in terms of alignment (coincident with the TiO_2 [001] crystallographic direction) and V–O angle of the FS peaks. However, STM images of the same system⁴⁷ clearly show that NCs are not symmetric along the [001] crystallographic direction and appear as two protrusions with different apparent height (see Figure S1). Thence, the only NC model compatible with the whole set of experimental data is V_4O_6 , since V_4O_8 is symmetric with respect to the substrate. It is also important to point out that the model we propose for V_4O_6 matches both the lateral dimensions of the asymmetric NCs observed by STM on the same system (6 Å along the [001] direction with two distinct protrusions, see Figure S1).

The electronic density of states (DOS) of V_4O_6 , and V_4O_8 supported NCs, is shown in Figure 4. All the systems are

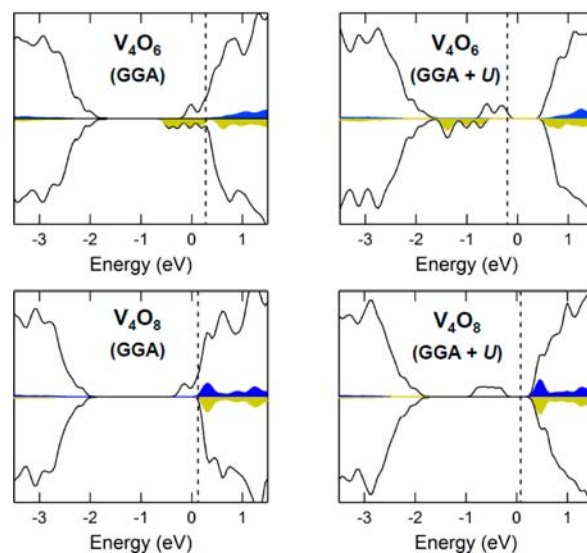


Figure 4. DOS of the V_4O_6 and V_4O_8 NCs. Dashed lines mark the Fermi level. Solid lines represent the total DOS including the NCs and the six topmost atomic layers of the slab. Filled blue/yellow areas indicate spin up/down vanadium partial DOS.

characterized by a NC \rightarrow surface electron transfer, whose extent can be deduced from the difference between the total charges of the surface with and without the NCs. This charge transfer was evaluated by summing the Löwdin charges of all the surface atoms. With the GGA+*U* (GGA) approach results are 0.71 (0.59) e and 0.69 (0.53) e for the V_4O_6 , and V_4O_8 case, respectively. As the charge transfer is larger for the most reduced clusters, it compensates the intrinsic differences in the population of the vanadium d levels of the NCs. A comparison between the DOS simulation and the VB spectra reported in Figure 1d rules out the V_4O_8 structure, whose DOS does not show any populated state around 1.0 eV, whereas it is in good

agreement with the V_4O_6 NC, once again validating the proposed model.

Interestingly the transferred electron is largely delocalized in the whole substrate (on a Ti site the maximum electron density increase is lower than 0.1 electron). Preferred sites are however the 5-fold Ti ions and the second-layer Ti ions in the same $\{010\}$ vertical planes.

Moreover, on the basis of a Löwdin analysis, we computed the following average charges: Ti = +0.82, V(V=O) = +0.61, V(V-O-V) = +0.74. Surprisingly the vanadium atoms bonded to terminal O (i.e., vanadyl species) are more reduced. If we consider that the oxidation number of Ti ions is 4+, we can infer that the oxidation state of vanadium is close to the formal V^{III} value.

The V_4O_6 model is quite interesting because it has no bulk counterpart: though it holds vanadyl groups, their oxidation state is not $V^{(V)}$. Moreover, V ions have different coordination: 2 of them are 4-fold, while the others are 3-fold coordinated by oxygen. Furthermore, the DOS curves discussed above show that the V atoms of V_4O_6 contribute both to filled and empty states close to the Fermi level. These interesting features prompted us to explore the reactivity of the NCs toward methanol.

A TPD-XPS analysis of the methanol desorption process from $VO_x(0.3 \text{ ML})/\text{TiO}_2(110)$ has been undertaken: we dosed deuterium labeled methanol (CH_3OD) as an aid to the analysis of the desorption pattern. Figure 5a shows methanol, formaldehyde and labeled water (D_2O) TPD peaks acquired after 2.0 L CH_3OD dosing at 130 K.⁵⁹ D_2O ($m/z = 20$) starts to desorb at about 230 K, and the peak maximum is located at 280 K. Formaldehyde ($m/z = 30$) signal, obtained after an accurate subtraction of the cracking pattern due to methanol, shows a clear peak at 300 K and proves the MODH reaction. Both $m/z = 31$ (CH_2OH^+ , obtained after the subtraction of the cracking pattern due to deuterated methanol) and $m/z = 32$ (CH_2OD^+) desorption peaks are present, and their maxima are located at higher temperature (about 330 K).

The analysis of methanol desorption from the same system, performed monitoring C 1s XPS peak evolution as a function of temperature (Figure 5b,c), gives us complementary information. We dosed a small amount of methanol (2.0 L), to avoid multilayer condensation. The C 1s photoemission line (Figure 5b,c) shows a broad peak centered at about 287 eV. After multicomponent analysis (see Figure 5b), four peaks can be identified in the 200–480 K range: at 286.9 (main peak, about 60% of the C 1s signal), 287.3, 288.6, and 285.2 eV. The first three can be ascribed to methoxy, molecular methanol, and formaldehyde, respectively.^{60,61} The origin of the peak centered at 285.5 eV is unclear, it can be connected either to a small C contamination on the sample surface or, more likely, to CH_xO (formyl) species adsorbed on different active sites.⁶⁰ Figure 5c displays the C 1s XPS peaks collected at increasing temperature in the 130–580 K range after a 2.0 L methanol dosing. The observed progressive negative BE shift of the peaks centroid is due to disappearance of the methanol–methoxy interaction.^{60,61} Figure 5d shows the trend of these components as a function of temperature. The intensity of the methoxy peak decreases monotonically, whereas the methanol peak shows a maximum between 200 and 300 K. Formaldehyde and CH_xO are only minor components, although the former shows a maximum in the same temperature range reported above.

By combining XPS and TPD data, we can hypothesize the following reactions:

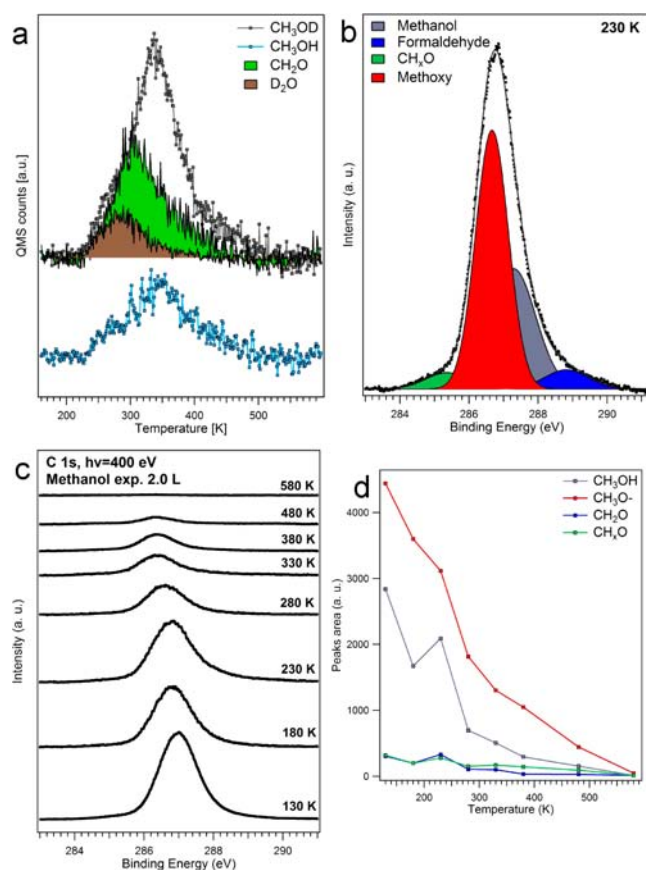
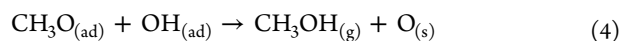
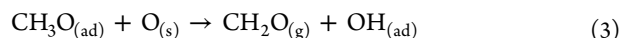


Figure 5. (a) TPD data showing the methanol, formaldehyde and deuterated water desorption peaks acquired after a 2.0 L methanol dosing at LT; (b) example of C 1s peak separation into single components; (c) C 1s XPS peak collected at different temperatures (130–580 K) after 2.0 L methanol dosing at LT; (d) C 1s peak components (from peak deconvolution) reported as a function of temperature.



Methanol dissociates on the VO_x -NCs forming methoxy and hydroxyls (reaction 1), as confirmed by C 1s peak multicomponent analysis. When the temperature is increased, surface hydroxyls ($\text{OD}_{(\text{ad})}$ either on VO_x -NCs or on the TiO_2 surface) can recombine to yield water (D_2O), as demonstrated by TPD spectra. Then the methoxy decomposes and desorbs as formaldehyde by transferring a proton to a surface oxygen ($\text{O}_{(\text{s})}$), which has been made available by reaction 2 either on NCs or TiO_2 (reaction 3).⁶² Since reaction 3 produces $\text{OH}_{(\text{ad})}$, a competitive reaction path involving the recombination of methoxy species with hydroxyls to form nondeuterated methanol (reaction 4) becomes active, as demonstrated by the temperature sequence of TPD peaks (i.e., formaldehyde desorbs at lower temperature than methanol). Finally, one has to take into account that on the TiO_2 areas not covered by VO_x -NCs, CH_3OD can be produced directly by recombinative desorption. This explains the high intensity and broad shape of the CH_3OD peak observed by TPD. By dosing methanol at low

temperature on the sample surface we investigated a stoichiometric reaction between the $\text{VO}_x/\text{TiO}_2(110)$ system and the adsorbates. The role of VO_x NCs can be revealed by V 2p_{3/2} peaks acquired before and after methanol desorption (Figure S3): a clear reduction from $\text{V}^{(\text{III})}$ to $\text{V}^{(\text{II})}$ is observed as indicated by the increase of the peak shoulder at 513.4 eV as a consequence of reaction 2. On the contrary, the Ti 2p spectrum is unaffected. These data suggest that the methanol dehydrogenation proceeds through a Mars van Krevelen mechanism,⁶³ and the titania substrate is mostly a spectator.

By considering the carbon mass balance of all the reactions, we determined a 25% conversion yield of adsorbed methanol to formaldehyde, which is twice the value observed on a clean $\text{TiO}_2(110)$ substrate treated at 473 K in a 5.0×10^{-8} mbar of oxygen background (Figure S4) and much more selective, since no other carbon related species is formed (on the contrary on clean TiO_2 , CO_2 is formed as well.).

To summarize, TPD and XPS data indicate that the V_4O_6 -NCs show an intrinsic reactivity and selectivity toward the MODH at LT (about 300 K). This low-temperature path has not been reported previously for conventional vanadia catalysts supported on titania,⁶⁴ ceria,⁶⁵ or silica,⁶⁶ where a temperature higher than 500 K is generally required for this reaction. On the other hand, vanadia monomers on ceria can decompose methanol to formaldehyde at 370 K.²³ In this latter case, the reason for this high reactivity has been traced back to the electronic interaction with the ceria substrate that can stabilize reduced states of the vanadia catalyst. The vanadia/titania system is only partially similar. As already discussed, our GGA +*U* calculations indicate that TiO_2 can efficiently accept extra electrons from vanadia NCs but in an almost constant value, i.e., 0.79, 0.70, and 0.69 e corresponding to V_4O_4 , V_4O_6 , and V_4O_8 , respectively. Surprisingly, the increase in the V 3d population in most reduced clusters does not lead to a significantly larger electron transfer. This provides a first indication that the same microscopic mechanism at work on VO_x/CeO_2 is not possible on TiO_2 , and the extra charge connected to the oxygen vacancy formation remains in the vanadia NCs. This is also verified experimentally: after methanol oxidation we observed new reduced species in the V 2p spectrum, whereas the Ti 2p photoemission peak remains oxidized. To confirm this view we have computed using GGA +*U* methods, the formation of an oxygen vacancy in the V_4O_6 tetramer (formally $\text{V}_4\text{O}_6 \rightarrow \text{V}_4\text{O}_5 + 1/2 \text{O}_2$), which is commonly used as a good descriptor of the catalytic activity.^{23,32,33} We obtained a value of 2.6 eV, which is lower than the oxygen defect formation energy on the substrate (above 3.5 eV²⁶ using $U = 3$ eV) and on the $\text{V}_2\text{O}_3(0001)$ surface (3.56 eV⁶⁷ calculated using a simple GGA approach).

CONCLUSION

In conclusion, combining XPS, AR-PD, and DFT calculations, we have demonstrated that when submonolayer amounts of V are deposited onto rutile $\text{TiO}_2(110)$ in a reactive O_2 environment, VO_x NCs are obtained. Furthermore, we have shown that mononuclear VO_x -NCs have a strong tendency to aggregate into polynuclear structures, which exhibit a high stability. The combination of experimental results (STM, XPS, and AR-PD) and DFT calculations has allowed us to find the structure of these VO_x NCs, which are asymmetric V_4O_6 tetramers aligned along the TiO_2 substrate [001] crystallographic direction. These exotic structures not only can be the active species in real catalytic systems but can also be used as

models to develop new molecular catalysts.⁶⁸ As a matter of fact, TPD and XPS have showed that V_4O_6 -NCs are extremely active and selective toward MODH reaction to yield formaldehyde at an unprecedented low temperature. The high catalytic activity has been traced back to the stabilization of the vanadia clusters with different oxidation states on the titania surface (V_4O_6 -NCs can accommodate oxygen vacancies easily at low energy cost, 2.6 eV), however no direct involvement of the substrate (i.e., reduction) during the reaction has been observed.

EXPERIMENTAL SECTION

XPS and AR-PD were performed at the ALOISA beamline (ELETTRA Synchrotron, Trieste, Italy).⁶⁹ XPS spectra were acquired in normal emission mode, using a photon energy of 400 eV for C 1s and 650 eV for V 2p, O 1s and Ti 2p.

The AR-PD intensity $I(\theta, \varphi)$ was measured for polar angles θ up to 68° and for azimuthal angles φ over a range of about 130° , including the two symmetry directions [001] and [1 $\bar{1}$ 0]. The X-ray beam was impinging at grazing incidence of 4° , and the light polarization was normal to the surface.

The AR-PD calculations for each model have been performed with the MSCD package,⁷⁰ multiple scattering order of 6, and a Rehr-Albers order of 2.

TPD experiments were collected in a multitechnique chamber equipped with a Quadrupole mass spectrometer, LEED, and XPS. The sample was cooled down to ~ 110 K, and TPD were recorded with $\beta = 2$ K/s up to 600 K.

Theoretical calculations were carried out with the PWSCF code, which is part of the Quantum-ESPRESSO (QE) suite,⁷¹ and it is a plane-wave pseudopotential implementation of the DFT. For further information see Supporting Information.

ASSOCIATED CONTENT

Supporting Information

STM image of VO_x -NCs on $\text{TiO}_2(110)$, TPD data of methanol desorption from the bare $\text{TiO}_2(110)$ substrate, DF simulated NCs models, V 2p XPS and experimental and computational details. This information is available free of charge via the Internet at <http://pubs.acs.org/>.

AUTHOR INFORMATION

Corresponding Author

stefano.agnoli@unipd.it

Notes

The authors declare no competing financial interest.

ACKNOWLEDGMENTS

This work has been funded by the Italian Ministry of Instruction, University and Research (MIUR) through the FIRB Project RBAP115AYN "Oxides at the nanoscale: multifunctionality and applications", and through the fund "Programs of national relevance" (PRIN-2009). We thank Prof. F. P. Netzer for the STM measurements. Calculations have been performed at the LICC ("Laboratorio interdipartimentale di chimica computazionale") HPC facility of the Department of Chemical Sciences, University of Padua.

REFERENCES

- (1) Roozeboom, F.; Cordingly, P. D.; Gellings, P. J. *J. Catal.* **1981**, *68*, 464.
- (2) Wachs, I. E. *Catal. Today* **2005**, *100*, 79.
- (3) Romanyshyn, Y.; Guimond, S.; Kuhlbeck, H.; Kaya, S.; Blum, R. P.; Niehus, H.; Shaikhutdinov, S.; Simic-Milosevic, V.; Nilius, N.;

- Freund, H. J.; Ganduglia-Pirovano, M. V.; Fortrie, R.; Dobler, J.; Sauer, J. *Top. Catal.* **2008**, *50*, 106.
- (4) Dobler, J.; Pritzsche, M.; Sauer, J. *J. Am. Chem. Soc.* **2005**, *127*, 10861.
- (5) Shapovalov, V.; Metiu, H. *J. Phys. Chem. C* **2007**, *111*, 14179.
- (6) Kim, H. Y.; Lee, H. M.; Metiu, H. *J. Phys. Chem. C* **2010**, *114*, 13736.
- (7) Price, S. P.; Tong, X.; Ridge, C.; Shapovalov, V.; Hu, Z.; Kemper, P.; Metiu, H.; Bowers, M. T.; Buratto, S. K. *Surf. Sci.* **2011**, *605*, 972.
- (8) Baldychev, I.; Vohs, J. M.; Gorte, R. J. *Appl. Catal. A: General* **2011**, *391*, 86.
- (9) Feng, Z.; Cheng, L.; Kim, C. Y.; Elam, J. W.; Zhang, Z.; Curtiss, L. A.; Zapol, P.; Bedzyk, M. J. *J. Phys. Chem. Lett.* **2012**, *3*, 2845.
- (10) Feng, Z.; Lu, J.; Feng, H.; Stair, P. C.; Elam, J. W.; Bedzyk, M. J. *J. Phys. Chem. Lett.* **2013**, *4*, 285.
- (11) Stacchiola, D. J.; Senanayake, S. D.; Liu, P.; Rodriguez, J. A. *Chem. Rev.* **2013**, *113*, 4373.
- (12) Asaduzzaman, A. Md.; Krüger, P. *J. Phys. Chem. C* **2008**, *112*, 4622.
- (13) Biener, J.; Baumer, M.; Madix, R. J. *Surf. Sci.* **1999**, *432*, 178.
- (14) Wang, Q.; Madix, R. J. *Surf. Sci.* **2001**, *474*, L213.
- (15) Wong, G. S.; Kragten, D. D.; Vohs, J. M. *J. Phys. Chem. B* **2001**, *105*, 1366.
- (16) Wang, Q.; Madix, R. J. *Surf. Sci.* **2002**, *496*, 51.
- (17) Li, M.; Altman, E. *J. Phys. Chem. C* **2009**, *113*, 2798.
- (18) Weckhuysen, B. M.; Keller, D. E. *Catal. Today* **2003**, *78*, 25.
- (19) Hadjiivanov, K. I.; Klissurski, D. G. *Chem. Soc. Rev.* **1996**, *25*, 61.
- (20) Freund, H. J.; Pacchioni, G. *Chem. Soc. Rev.* **2008**, *37*, 2224.
- (21) Werncke, C. G.; Limberg, C.; Knispel, C.; Mebs, S. *Chem.—Eur. J.* **2011**, *17*, 12129.
- (22) Wachs, I. E. *Dalton Trans.* **2013**, *42*, 11762.
- (23) Ganduglia-Pirovano, M. V.; Popa, C.; Sauer, J.; Abbott, H.; Uhl, A.; Baron, M.; Stacchiola, D.; Bondarchuk, O.; Shaikhutdinov, S.; Freund, H. J. *J. Am. Chem. Soc.* **2010**, *132*, 2345.
- (24) Park, J. B.; Graciani, J.; Evans, J.; Stacchiola, D. J.; Ma, S.; Liu, P.; Nambu, A.; Fernandez Sanz, J.; Hrbek, J.; Rodriguez, J. A. *Proc. Natl. Acad. Sci. U.S.A.* **2009**, *106*, 4975.
- (25) Agnoli, S.; Reeder, A. E.; Senanayake, S. D.; Hrbek, J.; Rodriguez, J. A. *Nanoscale* **2013**, DOI: 10.1039/C3NR04623K.
- (26) Chrétien, S.; Metiu, H. *J. Phys. Chem. C* **2011**, *115*, 4696–4705.
- (27) Dinse, A.; Ozarowski, A.; Hess, C.; Schomäcker, R.; Dinse, K.-P. *J. Phys. Chem. C* **2008**, *112*, 17664.
- (28) Dinse, A.; Carrero, C.; Ozarowski, A.; Schomäcker, R.; Schlögl, R.; Dinse, K.-P. *ChemCatChem* **2012**, *4*, 641.
- (29) Paier, J.; Kropp, T.; Penschke, C.; Sauer, J. *Faraday Discuss.* **2013**, *162*, 233.
- (30) Penschke, C.; Paier, J.; Sauer, J. *J. Phys. Chem. C* **2013**, *117*, 5274.
- (31) Cavalleri, M.; Hermann, K.; Knop-Gericke, A.; Hävecker, M.; Herbert, R.; Hess, C.; Oestereich, A.; Döbler, J.; Schlögl, R. *J. Catal.* **2009**, *262*, 215.
- (32) Brázdová, V.; Ganduglia-Pirovano, M. V.; Sauer, J. *J. Phys. Chem. C* **2010**, *114*, 4983–4994.
- (33) Tanya K. Todorova, T. K.; Ganduglia-Pirovano, M. V.; Sauer, J. *J. Phys. Chem. C* **2007**, *111*, 5141–5153.
- (34) Yang, F.; Kundu, S.; Vidal, A. B.; Graciani, J.; Ramirez, P. J.; Senanayake, S. D.; Stacchiola, D.; Evans, J.; Liu, P.; FdezSanz, J.; Rodriguez, J. A. *Angew. Chem., Int. Ed.* **2011**, *50*, 10198.
- (35) Tada, H.; Jin, Q.; Nishijima, H.; Yamamoto, H.; Fujishima, M.; Okuoka, S.; Hattori, T.; Sumida, Y.; Kobayashi, H. *Angew. Chem., Int. Ed.* **2011**, *50*, 3501.
- (36) Bondarchuk, O.; Xin Huang, X.; Kim, J.; Kay, B. D.; Wang, L.-S.; White, J. M.; Dohnálek, Z. *Angew. Chem., Int. Ed.* **2006**, *45*, 4786.
- (37) Baron, M.; Abbott, H.; Bondarchuk, O.; Stacchiola, D.; Uhl, A.; Shaikhutdinov, S.; Freund, H. J.; Popa, C.; Ganduglia-Pirovano, M. V.; Sauer, J. *Angew. Chem., Int. Ed.* **2009**, *48*, 8006.
- (38) Khodakov, A.; Olthof, B.; Bell, A. T.; Iglesia, E. *J. Catal.* **1999**, *181*, 205.
- (39) Hofmann, A.; Ganduglia-Pirovano, M. V.; Sauer, J. *J. Phys. Chem. C* **2009**, *113*, 18191.
- (40) Sambti, M.; Dalla Negra, M.; Granozzi, G. *Thin Solid Films* **2001**, *400*, 26.
- (41) Kim, H. Y.; Lee, H. M.; Pala, R. G. S.; Metiu, H. *J. Phys. Chem. C* **2009**, *113*, 16083.
- (42) Shapovalov, V.; Fievez, T.; Bell, A. T. *J. Phys. Chem. C* **2012**, *116*, 18728.
- (43) Badlani, M.; Wachs, I. E. *Catal. Lett.* **2001**, *751*, 137.
- (44) Olah, G. A. *Angew. Chem., Int. Ed.* **2005**, *44*, 2636.
- (45) Guo, Q.; Xu, C.; Ren, Z.; Yang, W.; Ma, Z.; Dai, D.; Fan, H.; Minton, T. K.; Yang, X. *J. Am. Chem. Soc.* **2012**, *134*, 13366.
- (46) Phillips, K. R.; Jensen, S. C.; Baron, M.; Li, S.-C.; Friend, C. M. *J. Am. Chem. Soc.* **2013**, *135*, 574.
- (47) Agnoli, S.; Sambti, M.; Granozzi, G.; Castellarin-Cudia, C.; Surnev, S.; Ramsey, M. G.; Netzer, F. P. *Surf. Sci.* **2004**, *562*, 150.
- (48) For the well established structure of the TiO₂(110) surface please refer to Diebold, U. *Surf. Sci. Rep.* **2003**, *48*, 53.
- (49) Li, M.; Hebenstreit, W.; Diebold, U.; Tyryshkin, A. M.; Bowman, M. K.; Dunham, G. G.; Henderson, M. A. *J. Phys. Chem. B* **2000**, *104*, 4944.
- (50) Della Negra, M.; Sambti, M.; Granozzi, G. *Surf. Sci.* **2000**, *461*, 118.
- (51) Parteder, G.; Allegretti, F.; Surnev, S.; Netzer, F. P. *Surf. Sci.* **2008**, *602*, 2666.
- (52) Sawatzky, G. A.; Post, D. *Phys. Rev. B* **1979**, *20*, 1546.
- (53) Zimmermann, R.; Claessen, R.; Reinert, F.; Steiner, P.; Hufner, S. *J. Phys. Cond. Matter* **1998**, *10*, 5697.
- (54) Demeter, M.; Neumann, M.; Reichelt, W. *Surf. Sci.* **2000**, *454–459*, 41.
- (55) Granozzi, G.; Sambti, M. *Adv. Mater.* **1996**, *8*, 315.
- (56) The center of the 2π plots corresponds to the surface normal, the radial section displays a polar scan, the circular section an azimuthal scan, and the anisotropy is given by the corresponding colour scale.
- (57) Blanco-Rey, M.; Abad, J.; Rogero, C.; Mendez, J.; Lopez, M. F.; Martin-Gago, J. A.; de Andres, P. L. *Phys. Rev. Lett.* **2006**, *96*, 055502.
- (58) See discussion in ref 2 for the definition of formal V^(VI) oxidation state.
- (59) A 2.0 L CH₃OD dosing is enough to saturate the first adsorption layer.
- (60) Matolin, V.; Johaneck, V.; Skoda, M.; Tsud, N.; Prince, K. C.; Skala, T.; Matolinova, I. *Langmuir* **2010**, *26*, 13333.
- (61) Romanyshyn, Y.; Guimond, S.; Gobke, D.; Sturm, J. M.; Kuhlbeck, H.; Dobler, J.; Ganduglia-Pirovano, M. V.; Sauer, J.; Freund, H. J. *Top. Catal.* **2011**, *54*, 669.
- (62) Abbott, H. L.; Uhl, A.; Baron, M.; Lei, Y.; Meyer, R. J.; Stacchiola, D. J.; Bondarchuk, O.; Shaikhutdinov, S.; Freund, H. J. *J. Catal.* **2010**, *272*, 82.
- (63) Doornkamp, C.; Ponc, V. *J. Mol. Catal. A: Chemical* **2000**, *162*, 19.
- (64) Farfan-Arribas, E.; Madix, R. J. *Surf. Sci.* **2003**, *544*, 241.
- (65) Feng, T.; Vohs, J. M. *J. Catal.* **2004**, *221*, 619.
- (66) Feng, T.; Vohs, J. M. *J. Phys. Chem. B* **2005**, *109*, 2120.
- (67) Gobke, D.; Romanyshyn, Y.; Guimond, S.; Sturm, J. M.; Kuhlbeck, H.; Dobler, J.; Reinhardt, U.; Ganduglia-Pirovano, M. V.; Sauer, J.; Freund, H. J. *Angew. Chem., Int. Ed.* **2009**, *48*, 3695.
- (68) Werncke, C. G.; Limberg, C.; Knispel, C.; Mebs, S. *Chem.—Eur. J.* **2011**, *17*, 12129.
- (69) Verdini, A.; Krüger, P.; Floreano, L. In *Surf. Anal. Tech.*; Bracco, G.; Holst, B., Eds.; Springer GmbH: Berlin, 2013; Vol. 51, 217.
- (70) MSCD code is freely distributed by Chen, Y.; M. A. Van Hove; <http://electron.lbl.gov/mscdpack/mscdpack.html>; see also Chen, Y.; Garcia de Abajo, F. J.; Chasse, A.; Ynzuna, R. X.; P.Kaduwela, A.; VanHove, M. A.; Fadley, C. S. *Phys. Rev. B* **1998**, *58*, 13121.
- (71) Giannozzi, P.; Baroni, S.; Bonini, N.; Calandra, M.; Car, R.; Cavazzoni, C.; Ceresoli, D.; Chiarotti, G. L.; Cococcioni, M.; Dabo, I.; Dal Corso, A.; de Gironcoli, S.; Fabris, S.; Fratesi, G.; Gebauer, R.; Gerstmann, U.; Gougoussis, C.; Kokalj, A.; Lazzeri, M.; Martin-Samos,

L.; Marzari, N.; Mauri, F.; Mazzarello, R.; Paolini, S.; Pasquarello, A.; Paulatto, L.; Sbraccia, C.; Scandolo, S.; Sclauzero, G.; Seitsonen, A. P.; Smogunov, A.; Umari, P.; Wentzcovitch, R. M. *J. Phys.: Cond. Matter.* **2009**, *21*, 395502.